



## Micro-XRF analysis of Early Bronze Age gold artefacts from Dhaskalio, Keros<sup>☆</sup>

Kalliopi Tsampa <sup>a</sup>, Andreas G. Karydas <sup>a,\*</sup>, Myrto Georgakopoulou <sup>b,1</sup>, Michael J. Boyd <sup>b,c,d</sup>, Colin Renfrew <sup>c,1</sup>

<sup>a</sup> Institute of Nuclear and Particle Physics, NCSR “Demokritos”, 153 41, Agia Paraskevi, Attiki, Greece

<sup>b</sup> Science and Technology in Archaeology and Culture Research Center, STARC, The Cyprus Institute, Nicosia, Cyprus

<sup>c</sup> McDonald Institute for Archaeological Research, University of Cambridge, UK

<sup>d</sup> British School at Athens, Athens, Greece

### ARTICLE INFO

#### Keywords:

Early Bronze Age Cyclades  
Dhaskalio, Keros  
Gold artefacts  
platinum Group Mineral (PGM) inclusion  
Micro-XRF analysis  
XRF Quantification  
Curved artefact surfaces

### ABSTRACT

This study examines a small collection of nine (9) Early Bronze Age gold artefacts from Dhaskalio, a site within the Keros complex in the Cyclades, using in-situ micro-XRF at the archaeological museum of Naxos Island, Greece. These artefacts, part of a rare group of Cycladic goldwork from this period, present analytical challenges due to their small sizes and curved surfaces. The effect of the unknown inclination of the alloy surface with respect to the nominal geometry was theoretically and experimentally evaluated in quantitative micro-XRF analysis and maximum uncertainties were deduced. Our analysis revealed that the Dhaskalio artefacts consist primarily of natural, unalloyed gold. The detection of a platinum group mineral (PGM) inclusion in one sample suggested its alluvial origin from secondary placer deposits. Comparisons with gold artefacts from archaeological sites across the Balkans, the Aegean, Egypt, and the Middle East, dated from the Neolithic period (5th millennium BCE) to the onset of the Middle Bronze Age (ca. 2000 BCE), indicate general compositional similarities while also reflecting the variability typical of early goldworking traditions in these regions.

### 1. Introduction

Dhaskalio, a small islet located just 90 m from Keros in the central Cyclades, was an important Early Bronze Age (EBA) site, forming part of a broader archaeological landscape that includes Kavos, well-known for its “special deposits”, which contain a remarkable number of Cycladic figurines (Renfrew, 2013; Renfrew et al., 2022). Radiocarbon dating has revealed three distinct phases: Phase A (Early Cycladic IIA, 2750 – 2550 BCE), Phase B (Early Cycladic IIB, 2550 – 2400 BCE), and Phase C (Early Cycladic III, 2400 – 2250 BCE) (Renfrew et al., 2012). Despite its small size, Dhaskalio became a significant metallurgical centre, processing copper, lead, and gold. Although gold artefacts were scarce, with only nine small pieces found, reflecting the limited availability of gold in the Cyclades during that era compared to regions like Crete and the north-eastern Aegean (Branigan, 1974; Gale & Stos-Gale, 1981), this is the largest concentration of gold in the EBA Cyclades.

In the Cyclades, beyond Keros, only one gold bead with a secure

Early Bronze Age date has been identified from the cemetery at Phyr rhoges on Naxos (Papathanasopoulos, 1962) while several gold items from Neolithic contexts have also been reported (Zachos, 2007). Additionally, three gold artefacts of probable Middle Bronze Age I or II date have been discovered at Agia Irini on the island of Kea (Caskey, 1972; Overbeck, 1989).

Given the limited availability of metal sources in the Aegean and nearby regions, gold and other items found in the Cyclades during the Early and Middle Bronze Age were integral to the dynamic exchange networks that facilitated the circulation of various important raw materials (Legarra Herrero, 2014). The geographical structure of the Aegean promoted early travel, despite the limited naval technology of the time, positioning the region as a crucial intersection between trade networks connecting Europe and the Near East. The important EBA site of Poliochni, Lemnos, may have been a key site in the connection of northern gold sources with the south Aegean (Cultraro, 2009). The establishment and control of these networks go hand in hand with

<sup>☆</sup> This article is part of a special issue entitled: ‘Proceedings of ICAS-EMME 4’ published in Journal of Archaeological Science: Reports.

\* Corresponding author at: Institute of Nuclear and Particle Physics, NCSR “Demokritos”, 153 41, Agia Paraskevi, Attiki, Greece.

E-mail address: [karydas@inp.demokritos.gr](mailto:karydas@inp.demokritos.gr) (A.G. Karydas).

<sup>1</sup> We regret to note that Myrto Georgakopoulou, Colin Renfrew passed away before the publication of this paper.

significant sociopolitical changes in the Aegean, including the emergence of the earliest complex societies in Europe (Broodbank, 2000; Renfrew, 1972).

The rarity of gold in the southern Aegean necessitated its acquisition through long-distance trade networks, likely from auriferous regions such as Thasos, Thrace, and the Black Sea, where alluvial deposits of native gold are found (Branigan, 1974; Legarra Herrero, 2014; Williams and Ogden, 1994). Although some scholars suggest that gold extraction occurred in Siphnos during Archaic and Classical periods, there is yet no conclusive evidence of Early Bronze Age exploitation (Wagner et al., 1985). Potential additional sources of gold could include northwest Anatolia and the central Taurus Mountains (Branigan, 1974; Yener, 2000).

Systematic analytical studies of archaeological artefacts can allow a better understanding of how technological preferences evolved over time. In the case of the Dhaskalio gold artefacts, archaeometric research focuses on determining the chemical composition of the alloys, providing information into the materials used rather than their form or methods of manufacture. While this paper does not address stylistic or technological features, the compositional analysis can still reveal important information about production practices and preferences. More broadly, archaeometric investigations contribute to provenance studies, which are critical for tracing ancient trade routes or identifying the use of local sources thereby indirectly indicating the presence of specialized production centres or local workshops. More specifically, the analysis of the chemical composition of the gold alloy is not limited only to the identification and quantification of major elements, ie gold (Au), silver (Ag) and copper (Cu) but also to trace elements. The determination of the platinum group mineral series (PGMs: ruthenium (Ru), rhodium (Rh), palladium (Pd), osmium (Os), iridium (Ir), platinum (Pt)) – as inclusions or in solution –, as well as other representative elements, such as tin (Sn), increases the inter-element associations and so the possibility of providing a unique fingerprint (Guerra et al., 1999).

A range of advanced analytical techniques is employed to investigate gold artefacts, focusing on the analysis of major, minor, and trace elements, including PGMs. PIXE (Proton Induced X-ray Emission) has been widely employed for non-destructive elemental composition analysis and due to high spatial resolution of external microprobes (~40 µm) (Lemasson et al., 2015) is ideal for detailed examination of small regions like PGM inclusions or joining areas in artefacts. However, PIXE faces limitations in detecting trace elements such as platinum (below 0.1 wt %) due to spectral interference from gold (Guerra & Tissot, 2016), whereas the special configuration of PIXE-XRF setup developed by Guerra and Calligaro (Guerra & Calligaro, 2004) offered Limits of Detection (LoD) for Pt detection in gold at the order of 100 ppm.

In addition, Synchrotron radiation induced X-ray Fluorescence (SR-XRF) technique, has proven powerful in analysing fingerprint trace elements like Sb, Sn, Te, Pb, Pt, Pd, and Zn (Guerra et al., 2008; Vasilescu et al., 2011). Pt analysis using Double Dispersive X-Ray Fluorescence (D<sup>2</sup>XRF) achieves detection limits as low as 0.9 ppm (Radtke et al., 2016).

Currently, the combination of laboratory or in-situ laser ablation (pLA) with inductively coupled plasma mass spectrometry (LA-ICP-MS) offers the detection of a broad range of trace elements in gold alloys with exceptional analytical sensitivity (Kunze et al., 2023; Numrich et al., 2023). LA-ICP-MS is minimally invasive since the ablation creates a crater with a diameter of about 100 µm and 150 µm depth (Watling & Herbert, 1994). However, in this way the analysis of the ablated material provides more representative results of the gold alloy composition, considering the possibility that very few µm of the surface of the ancient gold alloy have been enriched in gold (Troalen et al., 2014).

X-ray fluorescence (XRF) analysis is widely used as a versatile non-invasive analytical tool for determining the elemental composition of gold artefacts. It provides rapid measurements of major elements, as well as detecting certain minor or trace elements like iron (Fe). Most importantly, portable XRF spectrometers further enhance the

application of this technique by enabling on-site analysis, which is undoubtedly useful in various field settings (Hauptmann et al., 2018; Legarra Herrero & Martinón-Torres, 2021; Kantarelou et al., 2015; Karydas et al., 2004; Pantazis et al., 2003). However, for accurate quantitative analysis, surface irregularities on artefacts must be accounted for, since quantitative results are affected by these surface effects (Trojek & Trojková, 2023).

The present study focuses on the application of micro-XRF method for analysing gold artefacts from the EBA Cyclades and to develop a methodology to overcome analytical uncertainties that may occur from artefacts' uneven surface.

## 2. Material and methods

### 2.1. Sample description

The Dhaskalio assemblage includes nine (9) Early Bronze Age II gold alloy artefacts (Fig. 1; table S1). These items comprise two wires, three beads, two foils, and two sheets. All gold finds from Dhaskalio are quite small and were primarily uncovered through flotation residue sorting, emphasizing the importance of meticulous recovery techniques in detecting small precious metal objects in settlements (Georgakopoulou, 2023; Renfrew et al., 2018). When comparing the discovery of gold artefacts from Dhaskalio to those from other major Cycladic settlements, it is important to account for possible variations in field recovery methods. Fig. 2 shows the areas where each artefact was found during the excavations on Dhaskalio. The following descriptions offer some clarifications on the form and manufacture of the objects as necessary background for the present study. They are not intended as a full and detailed study, which will follow in the final publication of the material currently in preparation.

**Wire 16211.** Dating to Phase B, this exceptionally thin gold wire was recovered from Trench H during the 2016–2018 excavations. Its diameter is less than 0.5 mm, and it is twisted several times, measuring a maximum length of 6.4 mm. The wire weighs less than 0.01 g.

**Wire 2386.** This thin wire fragment, characterized by its circular cross-section, was recovered from Trench B during the 2016–2018 excavations and dates to Phase B. It has a length of 7.7 mm, a thickness of 0.8 mm, and a maximum dimension of 9 mm, with a weight of 0.06 g.

**Bead 2559.** Consisting of four concentric wires with piercings on two sides, this bead was recovered from Trench C during the 2016–2018 excavations, dating to Phase B. Its length is 9 mm, its width is 8 mm, and each individual wire is approximately 0.7 mm thick, with a total weight of 0.5 g.

**Bead 2791.** This tube-shaped bead is made of foil wrapped around itself and was recovered from Trench C during the 2016–2018 excavations, dating to Phase B. It has a diameter of 1.9 mm, a maximum dimension of 2.5 mm, and weighs 0.03 g. This type of bead is quite common through the span of millennia since examples of typological parallels can be found in the South Aegean in Sissi (Crete) dating to 2000 BCE (Legarra Herrero & Martinón-Torres, 2021, pl. 4366a, 4366b) and from Early Iron Age Armenia (Kunze et al., 2023, pl. 36–38).

**Bead 12202.** This circular bead, made of sheet metal, was recovered from Trench I during the 2006–2008 excavations and dates to Phase B. The bead features a wide opening, with a diameter of 2 mm compared to its external diameter of 3.5 mm. The opening is not precisely centred, resulting in a width that varies between 0.8 and 1 mm. It weighs less than 1 g. Close contemporaneous parallels are known from the northeastern Aegean in Troy IIg (Blegen et al., 1950) and Poliochni Yellow (Bernabò-Brea, 1976), as well as from southwestern Bulgaria (Christov, 2008).

**Foil 8564.** Folded into a flattened tube and twisted to meet at the ends, this foil may also represent a bead. Recovered from Trench N during the 2016–2018 excavations, it dates to Phase B. The width of the folded parts is 1.6 mm, and its maximum dimension is 9 mm, weighing 0.1 g.

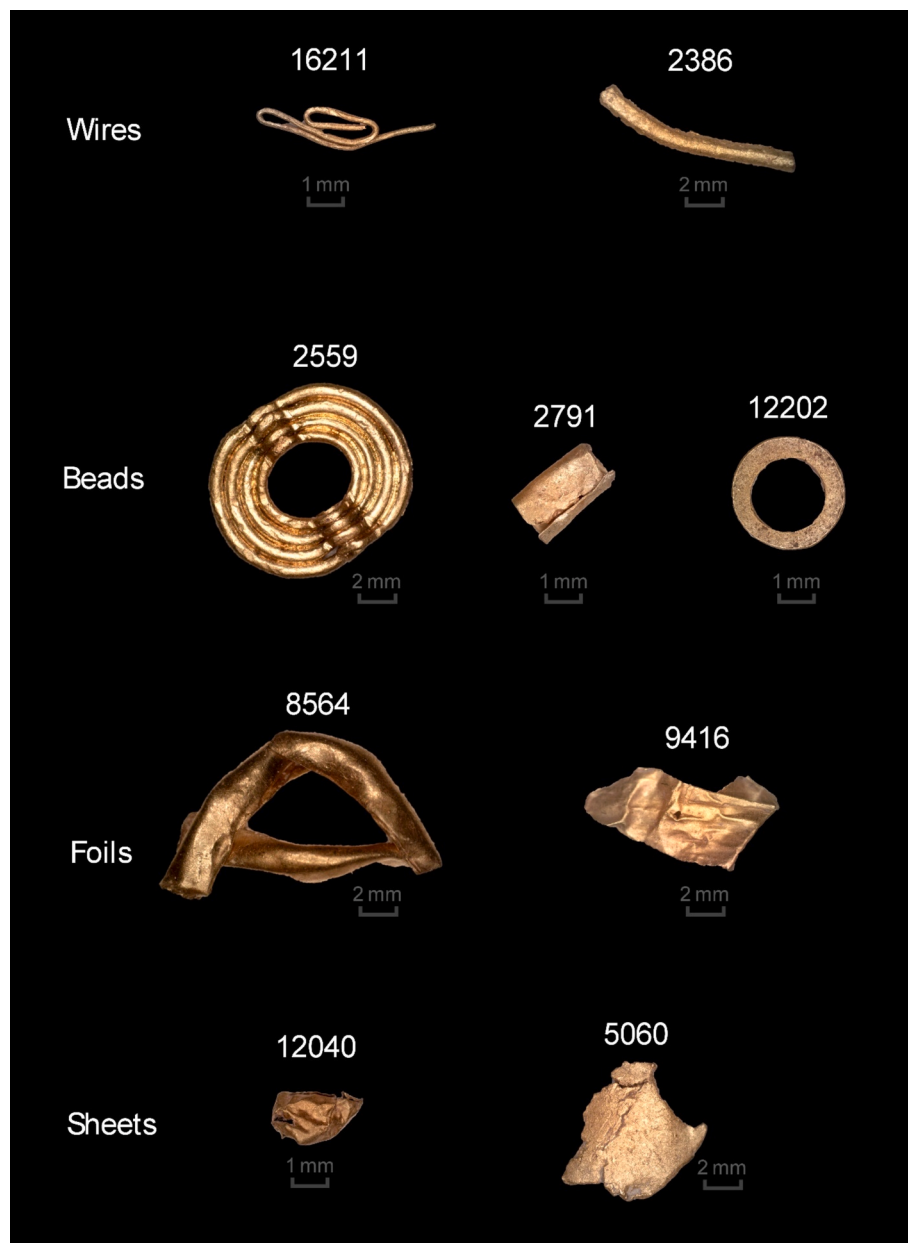


**Fig. 1.** Analysed gold artefacts from Dhaskalio (photos: Keros Project).

**Foil 9416.** A bent foil fragment recovered from Trench C during the 2016–2018 excavations, this artefact dates to Phase B. Its width measures 5 mm, with a maximum dimension of 8 mm, and it weighs 0.05 g.

**Sheet 12040.** Recovered from Trench A during the 2016–2018 excavations dating to Phase B, this artefact is a folded and squashed sheet-like fragment that may have originally been a bead. Its maximum dimension is 3 mm, and it weighs 0.012 g.

**Sheet 5060.** This minute fragment of gold sheet has one polished/shiny surface and one matte surface. It was recovered from Trench VI during the 2006–2008 excavations and dates to Phase C. The fragment measures 4 mm in length and weighs less than 1 g.

## 2.2. Micro X-ray Fluorescent (micro-XRF) analysis

The analysis of the gold artefacts was conducted at the archaeological museum of Naxos, Greece, using a customised version of Bruker Artax portable micro X-ray fluorescence spectrometer (micro-XRF) equipped with a micro-focus Rh-anode X-ray tube and polycapillary X-

ray lens offering a beam size at Cu-K $\alpha$  equal to  $\sim$ 50  $\mu$ m (under filtered excitation), as described in Kladouri et al. (2023).

In an area cleaned with an alcohol-soaked cotton pad, 5–8 independent spot measurements were conducted using the “line scanning” mode with a live time of 50 s acquisition time for each spot. For samples with strong surface convexities that prevented linear scans, individual spot measurements were taken with a live time of 300 s. The number and type of measurement (spot or line scan) conducted on each sample are presented in Supplementary table S2.1. It should be noted here that the reference irradiation geometry includes perpendicular incidence on the sample surface, whereas the exit angle of the fluorescence radiation towards the X-ray detector is 45 degrees. In all measurements, with the aid of the laser pointer at focus, special attention was given that the irradiated area was always viewed by the detector, thus excluding possible shading effects but without always being able to control and ensure the perpendicular incidence.

The accuracy of the applied analytical methodology was validated by analysing four international gold alloy Standard Reference Materials

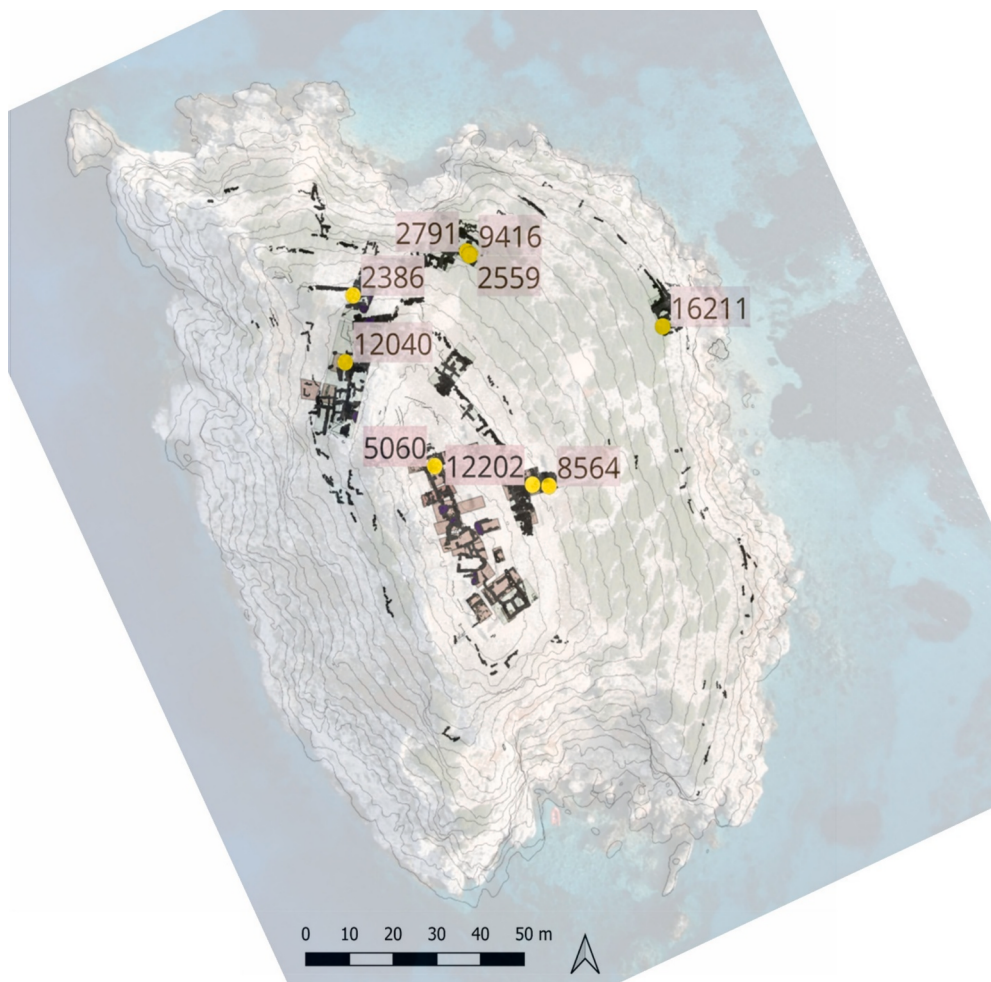


**Fig. 2.** The islet of Dhaskalio, with marked areas indicating where each artefact was discovered (photo: Keros Project).

(SRM), presented in Supplementary table S4. However, the micro-XRF technique faces challenges in accurately identifying certain trace elements such as platinum (Pt), lead (Pb), tin (Sn), palladium (Pd), and rhodium (Rh). These issues primarily arise from spectral interference: Pt is affected by the strong X-ray characteristic lines of gold (Au) and, to a lesser extent, lead (Pb), while the SnK $\alpha$  line interferes with the AgK $\beta$  characteristic line. The analysis of Pd is significantly hindered by the pronounced tailing of the frequently dominant Ag K $\alpha$  line in the spectrum. Additionally, it is affected by weak excitation due to the low-intensity, high-energy continuum transmitted through the lens. Furthermore, the strong presence of the Rh K $\alpha$  Rayleigh peak, originating from the tube's anode material, also limits the detection of Pd at trace levels. These interferences necessitate complementary techniques to confidently identify such trace elements in a gold matrix (Guerra & Calligaro, 2004; Numrich et al., 2023; Radtke et al., 2016). For elements detected in a gold matrix (using the ABSBL SRM for Cu, Ag, and Au, and sample 5060 for Pb), the Limits of Detection (LoD) are estimated for 300 s measurement time as follows: 0.03 wt% Fe; 0.02 wt% Cu; 0.17 wt% Ag; and 0.03 wt% Pb.

### 2.3. How does the curved shape of an object affect the analytical results?

The analytical challenges posed by the Dhaskalio artefacts arise primarily from their size and shape. These artefacts are on a millimetre scale with curved surfaces, which complicates the analytical process. During measurements, it was difficult to maintain constant and well-defined angles between the incident and detected beams relative to the sample, even if a micro-beam XRF setup was employed. Although the

small beam typically allows for easier selection of locations on the object that more closely resemble ideal flat and polished surfaces, commonly required for reproducible quantitative measurements, the irregular geometry of the artefacts remained an issue.

Gold alloys are composed only from detectable by XRF major and minor elements. However, even in this case, the sum of the PyMcada deduced elemental concentrations may not yield necessarily to 100 wt %, but rather to  $(100 \pm 5)$  wt %. Minor deviations could arise from geometrical aberrations from reference geometry, such as surface curvature or other irregularities at the point of analysis. Therefore, it is a common practice in XRF analysis to normalize the obtained experimental concentration to sum up to 100 wt %. When analysing a curved surface, as is the case for many Dhaskalio artefacts, the sum of the measured concentrations can range, for example, from as low as 50 wt% to as high as 150 wt%, resulting in inaccurate absolute results for the gold alloy composition. Ideally, knowing the exact angles of the incident and detected beams before the quantitative analysis would help eliminate these deviations, but in practice, this is rarely feasible.

The aim of this pilot study is to define the margins of possible uncertainties that may be introduced on the measured concentrations when an irregular gold alloy surface is analysed by micro-XRF. Curved surfaces pose a significant challenge in micro-XRF analysis as they can drastically affect the absolute characteristic X-ray intensities and their respective ratios, especially for more distant X-ray lines (Trojek, 2011). The angular dependence of the X-ray fluorescence intensity for a bulk material can be described by Geil and Thorne's model (2014).

Previous studies (Janssens et al., 2000; Trojek & Trojková, 2023) have demonstrated that when the X-ray beam size is smaller than surface

irregularities, such as convexities or concavities, the effect of these irregularities in X-ray transmission through a material resembles the effect of tilting a smooth surface in a certain direction. To investigate how surface curvature influences the count rate of characteristic X-rays, we have simulated the curvature of an artefact surface by rotating a flat, polished reference gold alloy (ABSBL), around a perpendicular axis that coincides with the incident beam direction and maintaining the normal vector of the surface co-planar with incident and outgoing beam directions.

The nominal concentrations (in wt%) of the ABSBL alloy are  $4.97 \pm 0.15$ ,  $5.04 \pm 0.15$ ,  $89.99 \pm 0.2$  for Cu, Ag and Au respectively, which closely match the ones determined in the artefacts from Dhaskalio.

The ABSBL reference material was mounted on a goniometer and placed on a height-adjustable platform, ensuring that both the tilting angle and the focal distance remained constant. The surface of the ABSBL sample was placed in such a way so that the normal to its surface belongs within the plane formed by the X-ray beam and the detector axis (Fig. 3a). The initial measurement was taken at the reference geometry, where the sample was aligned to form a  $90^\circ$  angle with the incident X-ray beam and a  $45^\circ$  angle with the detector axis.

Subsequent measurements involved inclination of the sample away from the detector around y-axis over a range of  $27^\circ$ , in increments of  $5^\circ$  from  $5^\circ$  to  $15^\circ$ , followed by increments of  $2^\circ$  (positive angles). Afterwards, the CRM was tilted towards the detector, starting again from the reference geometry, over a range of  $51^\circ$ , also in increments of  $5^\circ$  from  $5^\circ$  to  $15^\circ$ , followed by increments of  $2^\circ$  (negative angles). A total of 31 measurements were acquired, covering a tilt range of  $78^\circ$ . Each measurement was acquired for 200 s.

To validate these experimental results, XMI-MSIM simulation code was used, an open-source Monte Carlo simulation tool that predicts the spectral response of X-ray fluorescence spectrometers (Schoonjans et al., 2012). Simulations were performed with all relevant setup parameters such as beam energy distribution (Kantarelou & Karydas, 2016) and detector type to reproduce the dependence of the ABSBL reference gold alloy elements' fluorescence intensity at different surface inclination with respect to the reference geometry ( $90/45$  degrees for the incident/outgoing beams respectively).

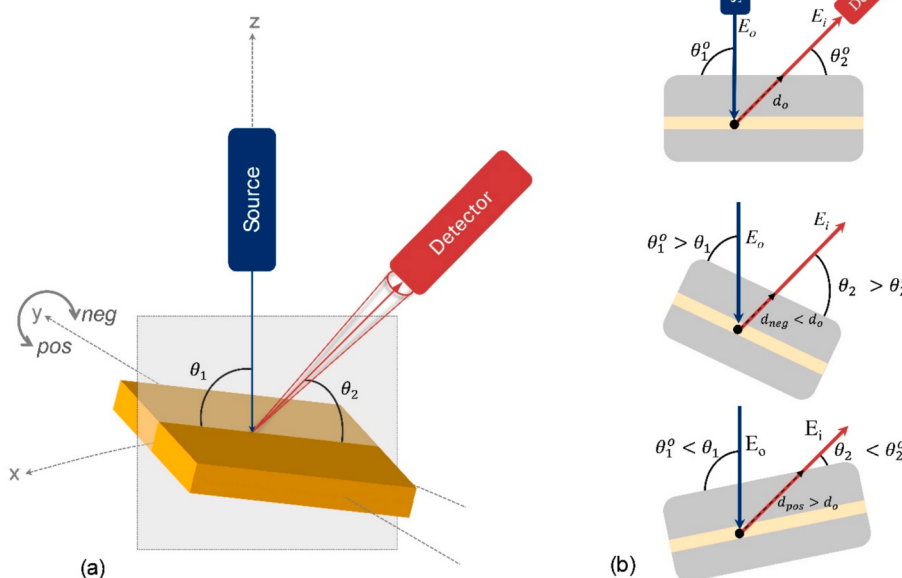


**Fig. 3.** (a) Schematic showing the arrangement of the incident beam, detector viewing angle, and the inclined surface of the certified reference material (CRM). (b) Visualization of the beam interaction volume and the travel paths ( $d_o$ ,  $d_{neg}$ ,  $d_{pos}$ ) of characteristic X-ray photons for three configurations: reference geometry, negative and positive inclination.

### 3. Results

#### 3.1. Evaluation of the influence of surface tilting on gold alloy

Fig. 4 presents the normalized count rates for the Cu K $\alpha$ , Ag K $\alpha$ , and Au L $\alpha$  X-ray characteristic lines in the ABSBL gold alloy, resulting from the tilting experiment. The tilting angle of  $0^\circ$  represents the reference geometry of  $90^\circ/45^\circ$ , with data shown for both experimental results and simulations. At positive tilting angles, the characteristic X-ray intensities decrease due to the longer path that the characteristic radiation produced in the matrix travels through the material, which results in greater photon absorption. In contrast, at negative angles, the shorter path length results in less absorption and subsequently to higher

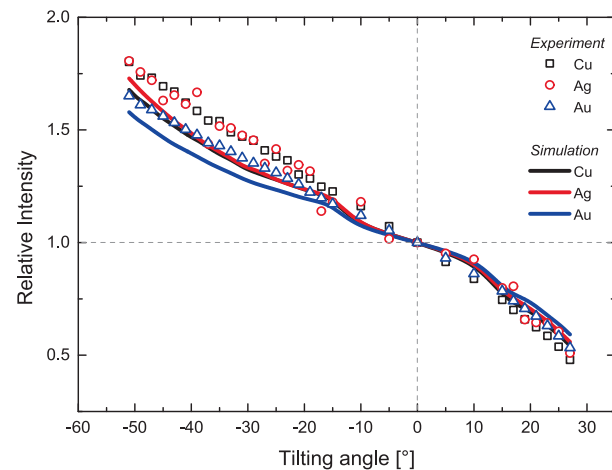


**Fig. 4.** Variation of X-ray count rates due to tilting of the ABSBL sample around the y-axis, for both experimental (open symbols) and XMI-MSIM simulation (lines) data. Positive angles indicate tilting around the y-axis away from the detector, while negative angles indicate tilting around the y-axis towards the detector.

characteristic X-ray intensities (Fig. 4b) (De Boer, 1989; Trojek, 2011). For a more comprehensive interpretation, it is important to note that self-attenuation effects at varying incident and exit angles are governed by the ratio of  $\sin\theta_1/\sin\theta_2$ , where  $\theta_1$  and  $\theta_2$  are the angles of incidence and detection, respectively, relative to the sample surface. The detected intensity emitted by element  $i$  is proportional to  $I(E_i) \propto 1/[\mu_s(\bar{E}_o) + \mu_s(E_i) \times (\sin\theta_1/\sin\theta_2)]$ , where  $\mu_s(\bar{E}_o)$  is the mass absorption coefficient of the sample at the effective incident energy ( $\bar{E}_o$ ), and  $\mu_s(E_i)$  is the mass absorption coefficient at the characteristic energy ( $E_i$ ) of element  $i$ . Among these terms, the ratio  $\sin\theta_1/\sin\theta_2$  is the dominant parameter shaping the detected intensity, particularly as it varies with the geometrical configuration of the measurement.

In the experimental results, positive tilting angles increased count rates for the Cu-K $\alpha$ , Ag-K $\alpha$ , and Au-L $\alpha$  lines by up to 50 %, 49 %, and 47 % at +27°, respectively, relative to the reference geometry. Negative angles led to decreases of -80 %, -81 %, and -65 % at -51° for these lines. In the XMI-MSIM simulated ABSBL sample, the positive tilting caused count rates to increase by 46 %, 44 %, and 41 % for Cu-K $\alpha$ , Ag-K $\alpha$ , and Au-L $\alpha$  lines at +27°. Negative angles showed reductions of -68 %, -73 %, and -58 % at -51°, with the XMI-MSIM simulation showing trends consistent with experimental data.

The measurement quantification was conducted through PyMca software (Solé et al., 2007) maintaining incident and take-off angles at 90°/45°. While the quantification analysis of each spectrum, adjusted to its actual geometry, yielded satisfactory results, keeping the geometry constant at 90°/45° ensures that any deviations from the nominal concentrations reflect the impact of the sample's inclination, as presented in supplementary table S5.

After applying normalization, the experimental concentrations (in weight percent, wt%) on extreme positions are reported in Table 1, showing deviations relative to the nominal values equal to 9 % for Cu, 18 % for Ag, and 1 % for Au, confirming the method's accuracy in compensating for surface irregularities.

The output of the XMI-MSIM simulations provides the X-ray peak counts (Cu-K $\alpha$ , Ag-K $\alpha$ , Au-L $\alpha$ ) for the elements that compose the gold alloy matrix. To convert those counts to elemental concentrations, calibration curves were employed as described by Karydas et al. (2004). The concentrations from the XMI-MSIM simulated tilting process, following normalization, were compared to those obtained under the reference geometry. The maximum deviations from the reference concentrations are 7.3 % for Cu, 5.5 % for Ag, and -0.7 % for Au.

### 3.2. The artefacts of Dhaskalio

#### 3.2.1. Gold alloys

Table 2 provides an overview of the calculated elemental composition for all analysed artefacts following normalization. The reported values represent the weighted averages of multiple individual measurements for each sample. The weighted uncertainties were calculated by considering the statistical error associated with each individual

**Table 1**  
Elemental concentrations (wt%) and their corresponding statistical uncertainties (%) of the ABSBL gold reference alloy material at reference geometry and under inclination after normalization.

Geometry	Concentrations [wt%]					
	Cu	s (Cu)	Ag	s (Ag)	Au	s (Au)
Reference geometry	4.96	0.77	4.70	3.42	90.35	0.21
Tilting in y-axis (away from the detector): +27°	4.52	0.53	4.53	2.43	90.95	0.15
Tilting in y-axis (towards the detector): -27°	5.20	0.46	5.14	2.25	90.66	0.14
Tilting in y-axis (towards the detector): -51°	5.34	0.40	5.12	1.78	89.54	0.12
ABSBL nominal concentrations	4.97	0.15	5.04	0.15	89.99	0.2

measurement. The detailed results of each measurement are provided in Supplementary Table S2.2. The results confirm that all artefacts are gold alloys, containing low concentrations of copper and varying levels of silver.

The gold content in the samples ranges from 74.8 wt% to 94 wt%. Silver is present in all samples, with concentrations between 5.8 wt% and 24.1 wt%. Copper is found in smaller amounts, with concentrations ranging from 0.09 wt% to 1.58 wt%.

Minor elements, including iron (Fe) and lead (Pb), were also detected. Iron concentrations were below 0.6 wt% in all samples. Lead was detected only in sample 5060 at approximately 0.1 wt%, though further investigation of two line scans on the sample revealed notable differences. The first line scan showed significant variations in Pb concentration, with several measurements falling below the detection limit, while the second line scan yielded consistent Pb results. The differences between the two scans suggest that the Pb may originate from burial contamination. Trace amounts of calcium were also found in all samples, likely originating from burial deposits.

The base metal composition was largely consistent across samples, with minimal variation in gold concentrations and moderate variation in silver. Specifically, gold concentrations deviated up to 1.5 % in sample 8564, while silver showed greater variability, reaching 7 % in sample 5060. Significant fluctuations were observed for iron (Fe) and copper (Cu), with deviations up to 50 % for Fe and 30 % for Cu across different measurements within each sample. These large fluctuations in Fe and Cu concentrations may reflect burial contamination, although primary alloy inhomogeneity cannot be excluded.

Measurements were also conducted to investigate the joining technique on artefact 2599. However, these measurements were assessed as non-reliable during evaluation due to the impact of shadowing effects and local morphology, except one, which is presented in the Supplementary material (Table S3).

#### 3.2.2. Platinum group mineral (PGM) inclusion

The accessible surface of all objects was carefully examined by digital microscopy (Dino-Lite) at different magnifications below the 100  $\mu\text{m}$  scale. However, due to the irregular shape and the morphology of several objects, like folded and twisted parts, the examination was restricted to a certain percentage of the alloy total surface. The result of this optical examination resulted in the detection of a platinum group mineral (PGM) inclusion of approximately 30  $\mu\text{m}$  diameter (Fig. 5), on artefact 12202. In this case, a dedicated analytical protocol was followed. More specifically, about 64 independent spot measurements were performed under the "area scanning" measurement mode with total acquisition live time of 360 s, using a 0.02 mm step between two consecutive measurements, covering a total area of 0.14 x 0.14  $\text{mm}^2$ . Elemental maps (Fig. 6) showing the distribution of PGM elements can be extracted through the analysis of the "area scanning" measurement. Furthermore, a spot measurement of 300 s, focused on the centre of the PGM inclusion was acquired (Fig. 6, left) and the semi-quantitative results are presented in Table 3. Since the beam size of the micro-XRF setup (~50  $\mu\text{m}$ ) is larger than the diameter of the PGM inclusion (~30  $\mu\text{m}$ ) also the major elements of the gold alloy are detected.

## 4. Discussion

### 4.1. Surface irregularities and quantification accuracy in Dhaskalio artefacts

The effect of the surface curvature in the quantification procedure of gold alloys was investigated to ensure the level of accuracy of our in-situ measurements and deduced concentrations on gold artefacts of complex shape.

Although the use of micro-XRF setups allows for more selective targeting of areas on the object that more closely resemble ideal flat and polished surfaces, challenges remain (Janssens et al., 2000).

**Table 2**

Elemental concentrations determined by micro-XRF analysis for the nine gold alloy artefacts from Dhaskalio. Reported values are weighted averages (wt%) with corresponding weighted statistical uncertainties (%).

Elements/ Inv. no.	Concentrations [wt%]									
	Fe	s(Fe)	Cu	s(Cu)	Ag	s(Ag)	Au	s(Au)	Pb	s(Pb)
2559	0.14	6.16	0.09	5.66	5.65	1.62	94.2	0.1	—	—
5060	0.48	2.19	0.40	1.38	5.91	1.14	93.7	0.1	0.09	5.52
8564	0.06	9.61	0.39	1.31	7.78	0.97	91.9	0.1	—	—
12040	0.11	6.63	0.47	1.32	10.2	0.9	89.3	0.1	—	—
16211	0.22	3.52	0.51	1.12	10.8	0.8	88.6	0.1	—	—
9416	0.48	2.90	0.49	1.50	19.0	0.8	80.6	0.1	—	—
2791	0.24	2.35	1.58	0.41	19.3	0.4	79.1	0.8	—	—
2386	0.17	3.11	0.25	1.37	23.2	0.4	76.4	0.1	—	—
12202	0.55	2.11	0.61	0.01	24.2	0.6	74.7	0.1	—	—

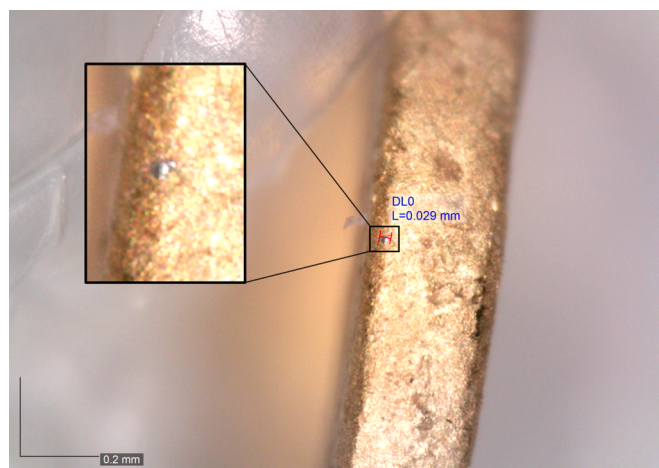


**Fig. 5.** Platinum group element mineral inclusion of artefact 12202. Photo by Dino-Lite handheld digital microscope (magnification x235).

Notwithstanding the influence of surface irregularities in XRF quantitation, it has been suggested that they do not impact the absolute concentrations of elements if normalization to 100 % is applied, as this procedure effectively corrects for these effects (Trojek & Trojková,

2023). The results of our experiment support this argument, since minimal discrepancies are observed regarding the reference geometry.

The detected X-ray intensities showed variations of the same order in both experimental and simulated results, though the experimental values were slightly higher. This discrepancy is likely due to imperfections in the experimental setup, which deviated from ideal conditions. A similar trend was observed in the variations of the elemental concentrations, where the experimental results were again somewhat elevated compared to the simulations.

A similar simulation method to the one applied to the ABSBL reference material was also employed for two artefacts from the Dhaskalio collection, which differ in their silver content. Simulations were conducted for sample 2386, containing 23.2 wt% silver, and sample 2559, with 5.65 wt% silver. Both samples have approximately the same copper concentration (<1%). The maximum deviations from the reference

**Table 3**

Semi-quantitative results (wt%) of PGM inclusion determined by means of micro-XRF analysis. The uncertainties refer to the percentage of statistical errors.

Concentrations [wt.%]	
Ru	9.3 ± 2.3
Os	69.1 ± 0.5
Ir	21.6 ± 1.0

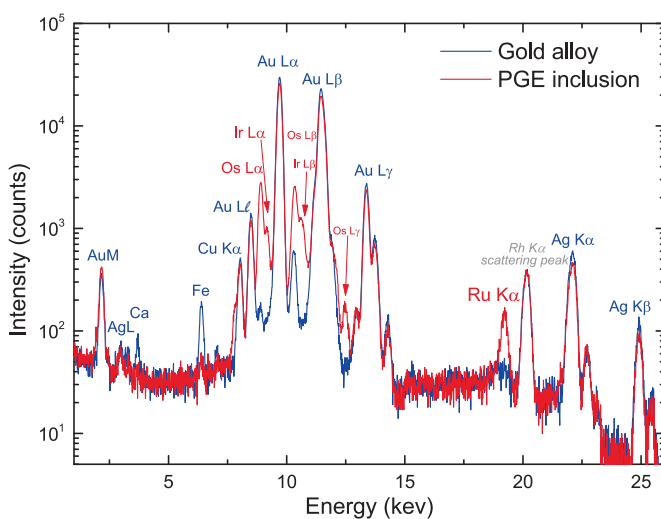


**Fig. 6.** Left: Comparison of micro-XRF spectra of PGM inclusion and gold alloy. Right: Os (up) and Ir (down) elemental maps. The colour scale on the right side of each map indicates the intensity (counts) of each element.

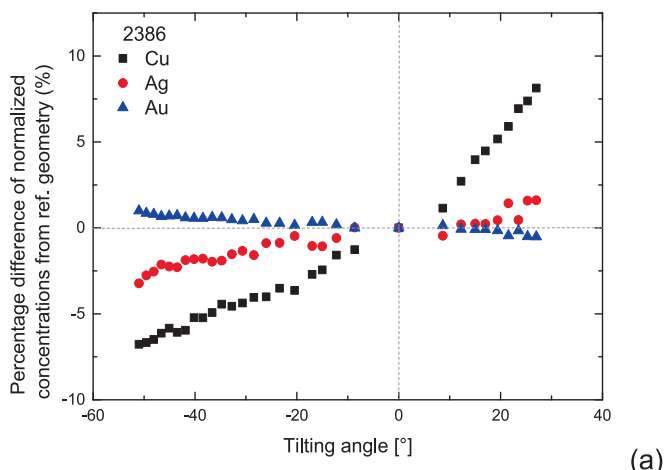
concentrations for both samples occurred at the extreme positive angle ( $27^\circ$ ). For sample 2386, the maximum deviations were 8.1 % for Cu, 3.2% for Ag, and 1.0 % for Au, while for sample 2559, the differences were 9.7 % for Cu, 5.7 % for Ag, and 0.4 % for Au. Fig. 7 presents the percentage differences between the concentrations obtained at each tilting angle of the XMI-MSIM simulation experiment and those from the reference geometry. These graphs demonstrate the impact of both normalization and surface tilting on the concentrations of a gold alloy. The observed differences are due to the relative abundance of each element within the alloy, since the higher the concentration of an element, the less significant the effect appears.

#### 4.2. Chemical composition and a broader comparison

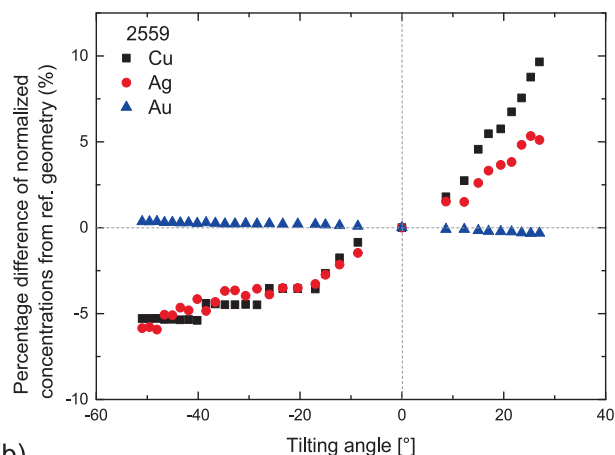
The chemical composition of the Dhaskalio artefacts is characterized by silver concentrations ranging from 5 % to 24 % and consistently low copper levels, mostly below 1 %. Copper concentrations fall within the expected range for natural unalloyed and unrefined gold, generally up to 2.5 % (Ogden, 1993), but typically under 1 % (Guerra & Calligaro, 2004), and in some cases even below 0.1 % (Pernicka, 2014). Silver values fall also within the documented variability of native gold sources, which may contain less than 1 wt% up to over 40 wt% Ag. Fig. 8 illustrates the metal colours associated with different compositional ranges and shows where each artefact falls within this chromatic spectrum. Based on their chemical composition, the artefacts can be divided into two distinct groups: Group A consists of five artefacts with lower silver concentrations (approximately 5–11 wt%), corresponding to yellow-toned hues; Group B includes four artefacts with higher silver content (ranging from 19–25 wt%), exhibiting green-yellow tones.

To develop a broader interpretive framework, gold artefacts from archaeological sites across the Balkans, the Aegean, Egypt, and the Middle East, dated from the Neolithic period (5th millennium BCE) to the onset of the Middle Bronze Age (ca. 2000 BCE), were considered. This framework allows for a comparison of the compositional elements, particularly silver and copper, which are the primary focus in most studies and publications. Fig. 9 presents these data, enabling comparisons across geographically and chronologically distinct contexts, including the Dhaskalio assemblage. In this comparison, only gold alloys with low Cu concentrations (<10 %) are considered. Although no clear patterns emerge, several observations can be drawn. While the Dhaskalio assemblage does not precisely match any cluster, there are notable overlaps between its compositions and the broader range observed in this comparative framework.

Group A artefacts from Dhaskalio (Ag 5–11 wt%, Cu < 1 wt%) are compositionally closest to Late Neolithic assemblages such as those from



(a)



(b)

**Fig. 7.** Simulation of the tilting procedure of (a) sample 2386 (Cu 0.25 wt%, Ag 23.2 wt%, Au 76.2 wt%) and (b) sample 2559 (Cu 0.09 wt%, Ag 5.65 wt%, Au 94.2 wt%). Percentage difference of concentrations for the three gold alloy elements from the concentrations derived at reference geometry.

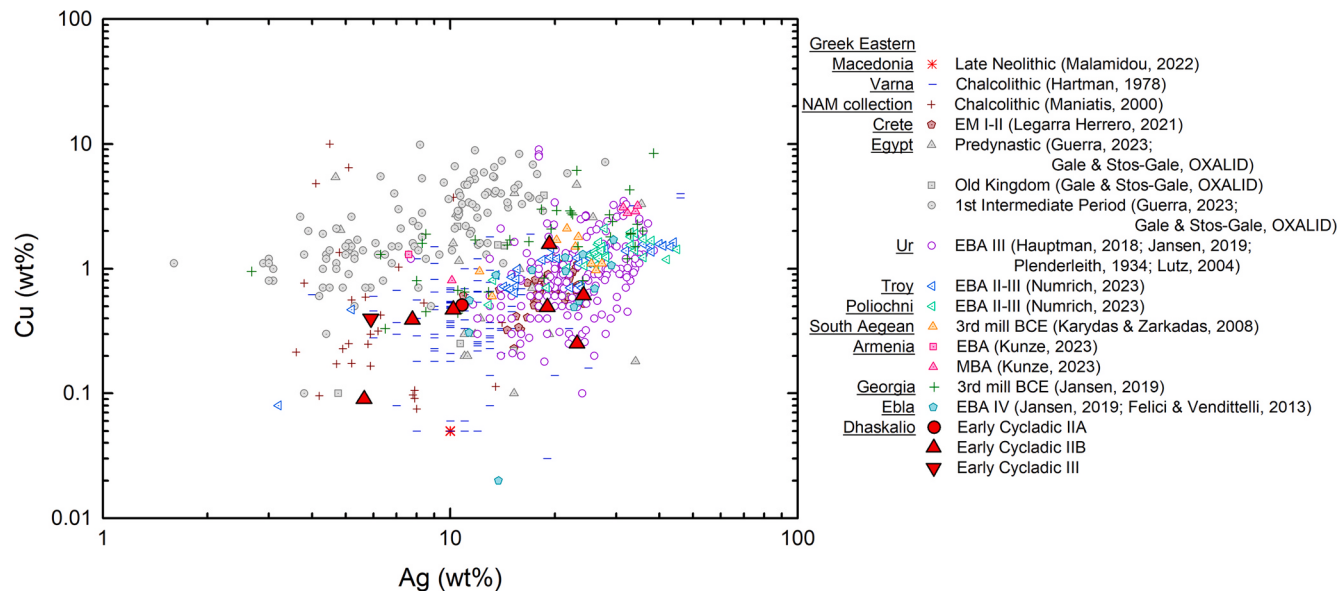


**Fig. 9.** Logarithmic scatterplot showing the levels of copper and silver in the Dhaskalio gold artefacts dated from the Early Bronze Age, compared to gold artefacts from archaeological sites across the Balkans, the Aegean, Egypt, and the Middle East, dated from the Neolithic period up to ~ 2000 BCE.

Predynastic period, including the beads from the diadem found at Abydos, dated to the Naqada II period (3900–3100 BCE), which contain the highest gold content at 98 wt% Au and 2 wt% Ag (Guerra et al., 2023), two from the Old Kingdom, and seventeen from the First Intermediate Period. Additional matches were identified in Georgia (8 artefacts), Ur (5), Troy and Poliochni (3), Ebla (2), South Aegean (2), MBA Armenia (1), Greek Eastern Macedonia (1), Crete (1).

Group B artefacts from Dhaskalio display silver levels in the range of 19–25 wt% Ag and maintain the low copper content (<1.6 wt%). This profile aligns more closely with Early Bronze Age gold artefacts from Mochlos (Crete), Troy and Poliochni (northern Aegean), and Ur (Mesopotamia). For instance, Early Minoan gold from Mochlos (3100–2200 BCE) exhibits silver concentrations of 10–33 wt%, commonly clustering around 19 wt%, and copper levels almost uniformly below 1 wt% (Legarra Herrero & Martinón-Torres, 2021). Troy and Poliochni artefacts (EBA II-III) show similarly elevated Ag and slightly higher Cu, and are described as being made from native gold, though the elevated amount of copper is unlikely to result from deliberate alloying (Numrich et al., 2023). The values shown for Troy and Poliochni in Fig. 9 refer only to the main body of the artefacts, excluding granulation or soldered sections. Artefacts from Ur (ca. 2450 BCE) span in general a wider compositional range, with some items reaching up to 40 wt% Cu; however, Fig. 9 focuses only on Ur's gold alloys with Au over 60 wt% (Hauptmann et al., 2018; Jansen, 2019). Group B artefacts from Dhaskalio fall directly within this compositional range, particularly with respect to Ag content, though they remain distinct due to their consistently low Cu levels. In the comparative dataset, within the broader range of Ag > 15 wt% and Cu < 1.6 wt%, 164 artefacts from Ur, 42 from Crete and 31 from Troy and Poliochni, exhibit similar silver concentrations while maintaining Cu below 1.6 wt%. Additional matches include 11 artefacts from Varna, 8 from Ebla, 7 from Egypt, and isolated examples from South Aegean (3) and Georgia (3) and Old Kingdom Egypt (1).

Regional comparisons further support potential associations with the Dhaskalio gold assemblage. Artefacts from Greek Eastern Macedonia (Dimitra and Dikili Tash, late 5th millennium BCE) show similar profiles of low Ag and Cu (Malamidou et al., 2022). In Dimitra, two beads were characterized by approximately 10 wt% Ag and 0.05 wt% Cu. The presence of quartz inclusions on the beads suggests minimal processing, indicating direct use of native gold. At Dikili Tash, four gold items (not shown in Fig. 9) were manufactured by hammering thin strips of gold

and also exhibited low silver content (4–9 wt%), consistent with natural alluvial sources and limited metallurgical intervention. Late 3rd millennium BCE material from Cape Kolonna (Aegina) (Karydas & Zarkadas, 2008) shows variable Ag values (12–27 wt%) and similarly low Cu (<2 wt%), again consistent with native gold use and are characterized as made from electrum. In contrast, Egyptian artefacts, particularly those from the First Intermediate Period, exhibit substantially greater variability. Some pieces contain over 50 wt% Ag and up to 50 wt% Cu, particularly in decorative items such as amulets (Guerra et al., 2023; Gale & Stos-Gale, Oxalid) indicating deliberate alloying or use of mixed-metal tools. Only artefacts with Au > 60 wt% from OXALID database (Gale & Stos-Gale, Oxalid) are included in Fig. 9.

Beyond the Aegean and Egypt, artefacts from Ebla (Early Bronze IV) and Georgia (mid-3rd millennium BCE) (Jansen, 2019) are characterized by silver contents up to 30 wt% and 40 wt%, respectively and copper up to 1 wt% and 8 wt%. Armenian material examined by Kunze et al. (2023) offers further information: one Early Bronze Age artefact contains Ag less than 8 wt% and Cu ~ 1 wt%, concentrations consistent with unrefined native gold, while four Middle Bronze Age artefacts show higher Ag (10–35 wt%) and moderate Cu (1–6 wt%), consistent with electrum, since no signs of intentional alloying were observed.

Overall, although the Dhaskalio assemblage is limited to just nine artefacts, Group A aligns well with earlier, unrefined Neolithic gold from southeastern Europe, while Group B overlaps compositionally with EBA artefacts from the Aegean and Mesopotamia. Both groups are notable for their consistently low copper content. The type of alloy used to manufacture the Dhaskalio artefacts appears to align with practices observed in other regions and is consistent with technological methods of the period.

The above comparison is valid strictly in relation to the gold metal compositional profile, without providing insights regarding the origin of the raw material. Provenance studies require targeted trace element analysis, to provide evidence about the type of gold metal (primary, secondary), and ideally, its geographical origin. Among the most useful indicators for alluvial (placer) gold are tin (Sn) and the platinum group elements (like Pt and Pd), which tend to remain stable during processing, like melting (Guerra, 2008). The ratio of platinum to palladium (Pt/Pd), in particular, has been proposed as a promising marker for distinguishing between gold sources and, in some cases, linking artefacts to specific placer deposits (Schlosser et al., 2012). However, XRF analysis of these trace elements using portable spectrometers suffers critically

from spectral interferences and it is rather restrictive below the analytical level of  $\sim 0.1$  wt%.

#### 4.3. Platinum group mineral inclusion

Platinum group mineral (PGM) inclusions in gold artefacts have long been recognised as indicators of geological origin, although they are not directly tied to specific regions or time periods (Jansen et al., 2016a; Young, 1972). Gold alloys with PGM inclusions originate from alluvial (placer) deposits, as Os-Ir-Ru inclusions are absent in primary gold deposits. In placer environments, gold and PGMs co-deposit due to their similar densities, making them inseparable by traditional extraction methods like panning.

PGM inclusions remain intact throughout metallurgical processes because they are insoluble in molten gold at temperatures below 1100 °C (Zwicker, 1998), which prevents them from melting or chemically altering during typical gold-working procedures. During gold smelting, gravitational separation often causes Os-Ir-Ru inclusion to settle at the bottom of moulds (Ogden, 1976), sometimes resulting in their presence near the surface of the final artefact. Because these inclusions are not altered, they provide information into ancient gold-processing techniques (Jansen et al., 2016a). Meeks and Tite (1980) note that variations in PGM inclusion concentrations within a single artefact likely reflect natural compositional differences from a single placer deposit rather than indicating multiple gold sources.

PGM inclusions are typically detected only when Pt concentration exceeds 100 ppm (Zaykov et al., 2018), as seen at sites like Ur in Mesopotamia (Jansen et al., 2016b). In placer deposits, Os-Ir-Ru inclusions form grains between 30–50 µm in size, though they can occasionally reach 100–150 µm (Zaykov et al., 2017).

The discovery of a platinum group mineral (PGM) inclusion in the gold artefact 12202 from Dhaskalio, composed of Os (69.1 wt%), Ir (21.6 wt%), and Ru (9.3 wt%), provides a basis for comparison with other gold findings containing similar inclusions. Fig. 10 compares the Os-Ir-Ru concentrations of Dhaskalio artefact 12202 with PGM inclusions identified in gold artefacts from Egypt, the Urals, and Ur. The Dhaskalio inclusion can be characterized as Os-rich and does not align clearly with any compositional cluster. Among the 183 PGM inclusions

considered in this comparative framework, only five exhibit higher Os concentrations than the one from Dhaskalio. Within the specific compositional range of Os > 60 wt%, Ir between 15–25 wt% and Ru < 10 wt%, only one comparable inclusion is identified, which originates from Ur, but this should not be seen as proof of a common origin.

The earliest reported examples come from the Chalcolithic Varna cemetery in Bulgaria where unrefined, native gold with minimal processing retained Os-Ir-Ru inclusions, attributed to placer gold sources (Leusch et al., 2015). Another early example is a diadem bead from Abydos which also preserves visible PGM inclusions (Guerra et al., 2023). In Mesopotamia, numerous Os-Ir-Ru(–Pt) inclusions were found in the gold assemblage of the Royal Tombs of Ur, suggesting the use of alluvial gold likely derived from placer deposits near ophiolitic zones in regions such as Afghanistan or Iran (Jansen et al., 2016a). The Dhaskalio inclusion thus chronologically follows these cases. Later examples of PGM inclusions are found in Egyptian goldwork dated from the Second Intermediate Period through the early 18th Dynasty (ca. 1800–1500 BCE) (Guerra & Pagès-Camagna, 2019; Lemasson et al., 2015; Troalen et al., 2014; Troalen & Guerra, 2016). These inclusions, often Os-Ir-Ru or Os-Ir-Ru-Pt alloys, are also associated with alluvial gold from the Eastern Desert or Nubia. It is worth noting that comparisons across different periods remain meaningful, since PGMs can persist even through recycling processes (Guerra, 2025). Much later, PGM-bearing inclusions have been identified in gold artefacts from the Urals and Siberia, dating from the Late Bronze Age to the Sarmatian period (ca. 1500 BCE–9th century CE), and linked to local placers derived from ultrabasic rocks (Zaikov et al., 2009). One of the earliest systematic surveys of such inclusions was conducted by Meeks & Tite (1980), who observed Os-Ir-Ru alloys in objects from the Near East and eastern Mediterranean spanning from 3200 BCE to 300 CE, reinforcing the association between PGM inclusions and the use of alluvial gold sources.

The absence of PGM inclusions in other artefacts does not necessarily indicate primary deposits as source material. As Meeks and Tite (1980) suggest, the lack of PGM inclusions on artefact surfaces may stem from several factors. Firstly, surface analysis or visual microscopic investigation typically examines only a small fraction of the total gold artefact, which may not fully represent the “true situation”. Additionally, PGM inclusions in the raw gold could have been removed by early refining

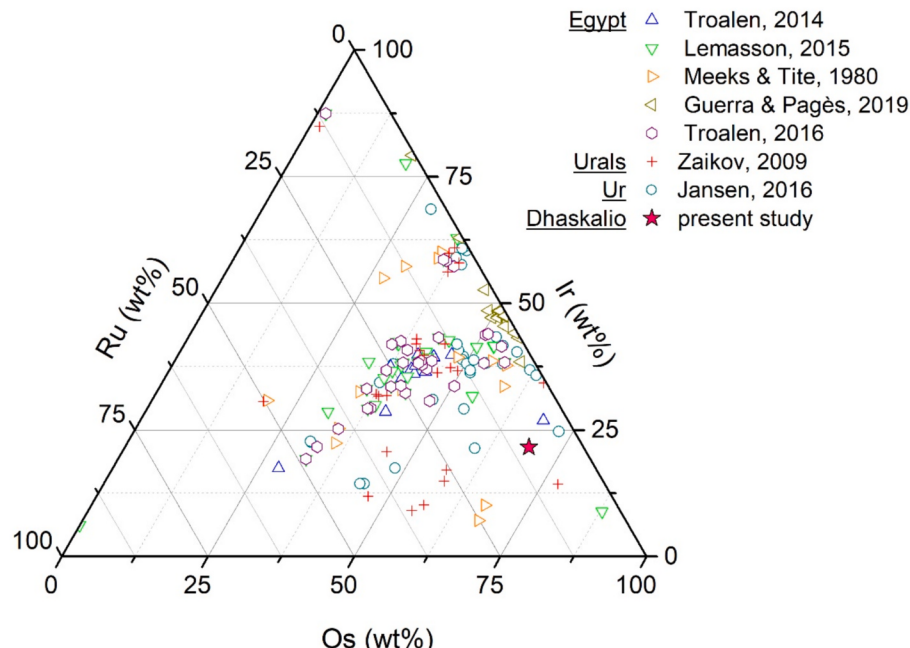


**Fig. 10.** Ternary plot showing the Os-Ir-Ru concentrations of the PGM inclusion in the Dhaskalio artefact 12,202 (red star symbol), compared with PGM inclusions identified in gold artefacts from Egypt, the Urals, and Ur.

methods, hand sorting, or gravity segregation of denser inclusions during melting. Lastly, the gold could originate from non-placer sources or from placer deposits naturally devoid in PGM inclusions. Current data are insufficient to support definitive assumptions, and a more sensitive analysis of certain trace elements (Pt, Pd, Sn) would be necessary to draw more reliable conclusions about the geological provenance of Dhaskalio gold. However, the presence of a single PGM inclusion in one artefact, the two distinct compositional groups formed amongst the Dhaskalio artefacts with similarities with respect to the earlier Varna gold and the contemporaneous Mesopotamia (Ur), provide evidence of extensive exchange networks that likely shaped the cultural and technological landscape of the Early Bronze Age Cyclades.

## 5. Conclusions

From the methodological point of view, the present study demonstrates the capability of micro-XRF as a non-destructive tool for analysing complex Early Bronze Age gold artefacts, such as those from Dhaskalio, where curved surfaces and small sizes present challenges for quantitative accuracy. The influence of surface curvature in quantitative micro-XRF analysis of gold objects was evaluated both theoretically and experimentally by rotating a flat, reference gold alloy. It has been shown that although significant changes in the count rates for major gold alloy elements are produced during tilting versus a reference geometry, the normalization condition, even at extreme tilting angle, provides with respect to the real concentration insignificant deviation for Au and less than 20 % and 10 % for Ag and Cu, respectively. These marginal deviations were further confirmed through simulation estimations of the tilting experiment.

The compositional analysis of the Dhaskalio gold artefacts identified gold-silver alloys with low copper concentrations, consistent with natural, unalloyed and unrefined gold. Notably, differences in Ag and Cu levels across samples suggest variations in raw material sources.

A key finding of this study was the detection of a platinum group mineral (PGM) inclusion, specifically an osmium-iridium-ruthenium (Os-Ir-Ru) alloy, in one of the Dhaskalio artefacts. The presence of this inclusion strongly indicates that the gold originated from placer deposits, where PGMs naturally occur alongside gold in alluvial environments.

## CRediT authorship contribution statement

**Kalliopi Tsampa:** Writing – original draft, Visualization, Validation, Methodology, Investigation, Formal analysis, Data curation. **Andreas G. Karydas:** Writing – review & Editing, Methodology, Investigation, Formal analysis, Data curation, Conceptualization. **Myrto Georgakopoulou:** Supervision, Resources, Project administration, Conceptualization. **Michael J. Boyd:** Writing – review & editing, Resources, Project administration, Funding acquisition, Conceptualization. **Colin Renfrew:** Writing – review & editing, Supervision, Funding acquisition, Conceptualization.

## Funding

This work was supported by the A. G. Leventis Foundation; the Stavros Niarchos Foundation; the Institute for Aegean Prehistory; the Balzan Foundation; the Packard Humanities Institute; the McDonald Institute for Archaeological Research; the Research and Innovation Foundation of Cyprus (EXCELLENCE/1216/0463); the Cyprus Institute; the British Academy; the Leverhulme Trust; the National Geographic Society; the Society of Antiquaries of London; the Gerda Henkel Stiftung; Cosmote; EZ-dot; Blue Star Ferries; Creta Farms; and private donors. Contributions were facilitated by Colin Renfrew, Michael Boyd, and Evi Margaritis.

## Declaration of Competing Interest

The authors declare that they have no known competing financial interests or personal relationships that could have appeared to influence the work reported in this paper.

## Acknowledgements

The Keros-Naxos Seaways Project was directed by Colin Renfrew and Michael Boyd for the British School at Athens, with associate director Irini Legaki. The fieldwork was conducted with the permission of the Hellenic Ministry of Culture and thanks are due to Ephorate of Antiquities of Cyclades director, Demetris Athanasoulis, and his many colleagues. Andreas Karydas is deeply grateful to the late Myrto Georgakopoulou for her confidence in our team and for inviting us to contribute to this work.

## Appendix A. Supplementary data

Supplementary data to this article can be found online at <https://doi.org/10.1016/j.jasrep.2025.105392>.

## Data availability

Data will be made available on request.

## References

- Bernabò-Brea, L., 1976. Poliochni II. Città preistorica nell'isola di Lemno: Vol. II,2. Blegen, C. W., Caskey, J. L., & Rawson, M. (1950). *Troy: Excavations conducted by the University of Cincinnati 1932-1938. I: The First and Second Settlements*. Princeton University Press.
- Branigan, K., 1974. *Aegean metalwork of the early and middle Bronze Age*. Clarendon Press.
- Broodbank, C., 2000. *An Island Archaeology of the Early Cyclades*. Cambridge University Press.
- Caskey, J.L., 1972. Investigations in Keos: part II: a conspectus of the pottery. *Hesperia: Journal of the American School of Classical Studies at Athens* 41 (3), 357–401.
- Christov, M. (2008). On the age of some gold artefacts from the Kraishte region in southwest Bulgaria. In R. Kostov, B. Gaydarska, & M. Gurova (Eds.), *Gearchaeology and Archaeomineralogy, Proceedings of the International Conference* (pp. 219–221). St. Ivan Ril.
- Cultraro, M., 2009. Crete and the islands of north Aegean before the palaces: reconsidering the evidence of Poliochni, Lemnos. In: MacDonald, C.F., Hallager, E., Niemeier, W.D. (Eds.), *The Minoan in the Central, Eastern and Northern Aegean – New Evidence*, Vol. 8. Monographs of the Danish Institute at Athens, pp. 219–242.
- De Boer, D., 1989. Angular dependencies of X-Ray Fluorescence Intensities. *X-Ray Spectrom.* 18, 119–129. <https://doi.org/10.1002/xrs.1300180309>.
- Gale, N.H. & Stos-Gale, Z.A., OXALID. ED XRF data for Bronze Age Greek, Cypriot and Egyptian gold and silver. Oxford Archaeological Lead Isotope Database (OXALID) database. Oxford: Isotrace Laboratory (<http://oxalid.arch.ox.ac.uk/>).
- Gale, N.H., Stos-Gale, Z.A., 1981. Cycladic lead and silver metallurgy. *Annual of the British School at Athens* 76, 169–224.
- Geil, E.C., Thorne, R.E., 2014. Correcting for surface topography in X-ray fluorescence imaging. *J. Synchrotron Radiat.* 21 (6), 1358–1363. <https://doi.org/10.1107/S160057751401875X>.
- Georgakopoulou, M., 2023. Different scales of archaeometallurgical research at the sites of Dhaskalio and Kavos on Keros: Site survey, excavations, and island-wide survey. In N. Nerantzi (Ed.), *Forging Values. Metals Technologies in the Aegean and Beyond from the 4th to the 1st Millennium BCE* (pp. 23–39). CReA-Patrimoine.
- Guerra, M. F. (2008). An overview on the ancient goldsmith's skill and the circulation of gold in the past: The role of x-ray based techniques. In *X-Ray Spectrometry* (Vol. 37, Issue 4, pp. 317–327). John Wiley and Sons Ltd. Doi: 10.1002/xrs.1013.
- Guerra, M.F., 2025. Goldworking in Mycenaean Thessaly: Technological study of the gold objects from the four tholos tombs in the Bay of Volos. *J. Archaeol. Sci.* 64. <https://doi.org/10.1016/j.jasrep.2025.105129>.
- Guerra, M.F., Calligaro, T., 2004. Gold traces to trace gold. *J. Archaeol. Sci.* 31 (9), 1199–1208. <https://doi.org/10.1016/j.jas.2002.05.001>.
- Guerra, M.F., Martínón-Torres, M., Quirke, S., 2023. *Ancient Egyptian gold, Archaeology and science in jewellery (3500–1000 bc)*. McDonald Institute for Archaeological Research.
- Guerra, M.F., Pagès-Camagna, S., 2019. On the way to the New Kingdom. Analytical study of Queen Ahhotep's gold jewellery (17th Dynasty of Egypt). *J. Cult. Herit.* 36, 143–152. <https://doi.org/10.1016/j.culher.2018.09.004>.
- Guerra, M.F., Radtke, M., Reiche, I., Riesemeier, H., Strub, E., 2008. Analysis of trace elements in gold alloys by SR-XRF at high energy at the BAMline. *Nucl. Instrum. Methods Phys. Res., Sect. B* 266 (10), 2334–2338. <https://doi.org/10.1016/j.nimb.2008.03.008>.

- Guerra, M.F., Sarthre, C.-O., Gondonneau, A., Barrandon, J.-N., 1999. Precious Metals and Provenance Enquiries using LA-ICP-MS. In *Journals of Archaeological Science* 26.
- Guerra, M.F., Tissot, I., 2016. Bronze Age and Iron Age gold torcs and earrings from the Iberian Atlantic façade: a non-invasive multi-analytical approach to the characterisation of the alloys and the corrosion. *X-Ray Spectrom.* 45 (1), 5–13. <https://doi.org/10.1002/xrs.2628>.
- Hartmann, A., 1978. Ergebnisse der spektralanalytischen Untersuchung aneolithischer Goldfunde aus Bulgarien. *Studia Praehistorica* 1, 27–45.
- Hauptmann, A., Klein, S., Paoletti, P., Zettler, R.L., Jansen, M., 2018. Types of Gold, Types of silver: the Composition of precious Metal Artifacts Found in the Royal Tombs of Ur, Mesopotamia. *Zeitschrift für Assyriologie und Vorderasiatische Archäologie* 108 (1), 100–131. <https://doi.org/10.1515/za-2018-0007>.
- Jansen, M., 2019. Geochemie und Archäometallurgie des Goldes der Bronzezeit in Vorderasien.
- Jansen, M., Aulbach, S., Hauptmann, A., Höfer, H.E., Klein, S., Krüger, M., Zettler, R.L., 2016a. Platinum group placer minerals in ancient gold artifacts - Geochemistry and osmium isotopes of inclusions in Early Bronze Age gold from Ur/Mesopotamia. *J. Archaeol. Sci.* 68, 12–23. <https://doi.org/10.1016/j.jas.2016.02.004>.
- Jansen, M., Hauptmann, A., & Klein, S., 2016. Where Does the Gold from the Cemetery of Ur Come From? –Provenancing Gold Sources Using Analytical Methods. In *The Royal Tombs of Ur, Mesopotamia* (Vol. 98).
- Janssens, K., Vittiglio, G., Deraedt, I., Aerts, A., Vekemans, B., Vincze, L., Wei, F., Deryck, I., Schalm, O., Adams, F., Rindby, A., Knöchel, A., Simionovici, A., Snigirev, A., 2000. Use of Microscopic XRF for Non-Destructive Analysis in Art and Archaeometry Vol. 29.
- Kantarelou, V., Karydas, A.G., 2016. A simple calibration procedure of polycapillary based portable micro-XRF spectrometers for reliable quantitative analysis of cultural heritage materials. *X-Ray Spectrom.* 45 (2), 85–91. <https://doi.org/10.1002/xrs.2661>.
- Kantarelou, V., Karydas, A.G., Sokaras, D., Mahfouz, L., Qurdab, A., Al-Saadi, M., Giannoulaki, M., Argyropoulos, V., 2015. In situ scanning micro-XRF analyses of gilded bronze figurines at the National Museum of Damascus. *J. Anal. At. Spectrom.* 30 (8). <https://doi.org/10.1039/c5ja0079c>.
- Karydas, A.G., Kotzamanis, D., Bernard, R., Barrandon, J.N., Zarkadas, C., 2004. A compositional study of a museum jewellery collection (7th-1st BC) by means of a portable XRF spectrometer. *Nucl. Instrum. Methods Phys. Res., Sect. B* 226 (1–2), 15–28. <https://doi.org/10.1016/j.nimb.2004.02.034>.
- Karydas, A.G., Zarkadas, Ch. (2008). Report on the XRF measurements at Piraeus Archaeological Museum. In C. Reinholdt (Ed.), *Der Frühbronzezeitliche schmuckhortfund von Kap Kolonna* (pp. 99–104).
- Kladouri, N.K., Skalta, S., Gerodimos, T., Pezouani, K., Karydas, A.G., 2023. Microscopic X-ray fluorescence analyses ( $\mu$ -XRF) of copper-based and silver alloy coins minted in Rhodes, Greece, from the fourth century BCE to the second century CE. *Archaeol. Anthropol. Sci.* 15 (9). <https://doi.org/10.1007/s12520-023-01834-0>.
- Kunze, R., Meliksetian, K., Lockhoff, N., Bobokhyan, A., Wolf, D., Davtyan, R., Simonyan, H., 2023. Prehistoric gold from Lake Sevan Basin? New research on Armenian gold deposits and objects. *J. Archaeol. Sci. Rep.* 52. <https://doi.org/10.1016/j.jasrep.2023.104267>.
- Legarra Herrero, B. (2014). The role of gold in south Aegean exchange networks (3100–1800 BC). In H. Meller, R. Risch, & E. Pernicka (Eds.), *Metalle der Macht – Frühes Gold und Silber / Metals of power – Early gold and silver*.
- Legarra Herrero, B., Martinón-Torres, M., 2021. Heterogeneous production and enchainment consumption: Minoan gold in a changing world (ca. 2000 BCE). *Am. J. Archaeol.* 125 (3), 333–360. <https://doi.org/10.3764/ajaa.125.3.0333>.
- Lemasson, Q., Moignard, B., Pacheco, C., Pichon, L., Filomena Guerra, M., 2015. Fast mapping of gold jewellery from ancient Egypt with PIXE: Searching for hard-solders and PGE inclusions. *Talanta* 143, 279–286. <https://doi.org/10.1016/j.talanta.2015.04.064>.
- Leusch, V., Armbruster, B., Pernicka, E., & Slavčev, V. (2015). On the invention of gold metallurgy: The gold objects from the Varna i cemetery (Bulgaria) - Technological consequence and inventive creativity. In *Cambridge Archaeological Journal* (Vol. 25, Issue 1, pp. 353–376). Cambridge University Press. Doi: 10.1017/S0959774314001140.
- Malamidou, D., Tsirtsoni, Z., Vaxevanopoulos, M., 2022. The emergence of metal use in Greek Eastern Macedonia during the Neolithic period (late 6 th-5 th millennia BC). *Documenta Praehistorica* XLIX, 10.4312/dp.49.6.
- Maniatis, Y., Karydas, A., Mangou, E., & Paradellis, T. (2000). *Scientific study of Neolithic gold periapts from the Greek National Archaeological Museum*.
- Meeks, N.D., Tite, M.S., 1980. The analysis of platinum-group element inclusions in gold antiquities. *J. Archaeol. Sci.* 7 (3), 267–275. [https://doi.org/10.1016/S0305-4403\(80\)80029-X](https://doi.org/10.1016/S0305-4403(80)80029-X).
- Numrich, M., Schwall, C., Lockhoff, N., Nikolentzos, K., Konstantinidi-Syvridi, E., Cultraro, M., Horejs, B., Pernicka, E., 2023. Portable laser ablation sheds light on Early Bronze Age gold treasures in the old world: New insights from Troy, Poliochne, and related finds. *J. Archaeol. Sci.* 149. <https://doi.org/10.1016/j.jas.2022.105694>.
- Ogden, J. (1993). Aesthetic and technical considerations regarding the colour and texture of ancient goldwork. In *Metal plating and patination* (pp. 39–49).
- Ogden, J.M., 1976. The So-called “platinum” Inclusions in Egyptian Goldwork. *J. Egypt. Archaeol.* 62 (1976), 138. <https://doi.org/10.2307/3856354>.
- Overbeck, J.C., 1989. *Ayia Irini: Period IV: Part 1: the Stratigraphy and the find deposits*. Philipp von Zabern.
- Pantazis, T., Karydas, A. G., Doumas, C., Vlachopoulos, A., Nomikos, P., & Dinsmore, M. (2003). *X-Ray Fluorescence Analysis of a Gold Ibex and other Artifacts from Akrotiri*.
- Papathanasiopoulos, G.A., 1962. Κοκλαδικά Νάζου. In *Αρχαιολογικόν Δελτίον* Vol. 17, 104–151.
- Pernicka, E., 2014. Possibilities and limitations of provenance studies of ancient silver and gold. *Metals of Power – Early Gold and Silver* 153–164.
- Radtke, M., Buzanich, G., Guilherme, A., Reinholz, U., Riesemeier, H., Scharf, O., Scholz, P., Guerra, M.F., 2016. Double Dispersive X-Ray Fluorescence (D2XRF) based on an Energy Dispersive pnCCD detector for the detection of platinum in gold. *Microchem. J.* 125, 56–61. <https://doi.org/10.1016/j.microc.2015.10.039>.
- Renfrew, C., 1972. *The emergence of civilization: the Cyclades and the Aegean in the third millennium BC*. Methuen & Company.
- Renfrew, C., 2013. The Sanctuary at Keros: questions of materiality and monumentality. *Journal of the British Academy* 1, 187–212.
- Renfrew, C., Boyd, M.J., Athanasoulis, D., Brodie, N., Carter, T., Dellaporta, K., Floquet, M., Gavalas, G., Georgakopoulou, M., Gkouma, M., Hilditch, J., Krijnen, A., Legaki, I., Margaritis, E., Marthari, M., Moutafí, I., Philaniotou, O., Sotirakopoulou, P., Wright, J., 2022. The sanctuary at Keros in the Aegean Early Bronze Age: from centre of congregation to centre of power. *Journal of Greek Archaeology* 7, 1–36. <https://doi.org/10.32028/jga.v7i.1779>.
- Renfrew, C., Boyd, M.J., Margaritis, E., 2018. Interdisciplinary approaches to the prehistory of Keros. *Archaeol. Rep.* 64, 67–84.
- Renfrew, C., Boyd, M.J., Ramsey, C.B., 2012. The oldest maritime sanctuary? Dating the sanctuary at Keros and the Cycladic Early Bronze Age. *Antiquity* 86 (331), 144–160. <https://doi.org/10.1017/S0003598X00062517>.
- Schlosser, S., Reinecke, A., Schwab, R., Pernicka, E., Sonetra, S., Laychour, V., 2012. Early Cambodian gold and silver from Prohear: Composition, trace elements and gilding. *J. Archaeol. Sci.* 39 (9), 2877–2887. <https://doi.org/10.1016/j.jas.2012.04.045>.
- Schoonjans, T., Vincze, L., Solé, V.A., Sanchez Del Rio, M., Brondeel, P., Silversmit, G., Appel, K., Ferrero, C., 2012. A general Monte Carlo simulation of energy dispersive X-ray fluorescence spectrometers - Part 5: Polarized radiation, stratified samples, cascade effects, M-lines. *Spectrochimica Acta - Part B Atomic Spectroscopy* 70, 10–23. <https://doi.org/10.1016/j.sab.2012.03.011>.
- Solé, V.A., Papillon, E., Cotte, M., Walter, P., Susini, J., 2007. A multiplatform code for the analysis of energy-dispersive X-ray fluorescence spectra. *Spectrochimica Acta - Part B Atomic Spectroscopy* 62 (1), 63–68. <https://doi.org/10.1016/j.sab.2006.12.002>.
- Troalen, L. G., Tate, J., & Guerra, M. F. (2014). Goldwork in Ancient Egypt: Workshop practices at Qurneh in the 2nd Intermediate Period. In *Journal of Archaeological Science* (Vol. 50, Issue 1, pp. 219–226). Academic Press. Doi: 10.1016/j.jas.2014.07.010.
- Troalen, L., Guerra, M.F., 2016. Gold from the tomb of Scribe Beri: a comparative analytical approach to the New Kingdom gold grave goods from Riqa (Egypt). *Appl. Phys. Mater. Sci. Process.* 122 (3). <https://doi.org/10.1007/s00339-016-9699-1>.
- Trojek, T., 2011. Reduction of surface effects and relief reconstruction in X-ray fluorescence microanalysis of metallic objects. *J. Anal. At. Spectrom.* 26 (6), 1253–1257. <https://doi.org/10.1039/c0ja00187b>.
- Trojek, T., Trojková, D., 2023. Uncertainty of Quantitative X-ray Fluorescence Micro-Analysis of Metallic Artifacts Caused by their Curved Shapes. *Materials* 16 (3). <https://doi.org/10.3390/ma16031133>.
- Vasilescu, A., Constantinescu, B., & Bugoi, R., 2011. *Micro-sr-xrf studies of gold provenance in archaeology*. <https://www.researchgate.net/publication/228757548>.
- Wagner, G., Pernicka, E., Seeliger, T., Özturnali, Ö., Baranyi, I., Begemann, F., Schmitt-Strecker, S., 1985. Geologische untersuchungen zur frühen metallurgie in NW-Anatolien. *Bulletin of the Mineral Research and Exploration Institute of Turkey* 101 (102), 45–81.
- Watling, R.J., Herbert, H.K., 1994. Gold fingerprinting by laser ablation inductively coupled plasma mass spectrometry. In *Spectrochimica Acta* Vol. 499, Issue 2.
- Williams, D., & Ogden, J. (1994). *Greek gold: jewellery of the classical world*.
- Yener, K., 2000. The Rise of Complex Metal Industries in Anatolia, Ancient Turkey. In *The Domestication of Metals* (Vol. 4, pp. 1–16). Brill.
- Young, W. I. (1972). The fabulous gold of the Pactolos Valley. *Boston Museum Bulletin: Museum of Fine Arts*, L(3).
- Zachos, K. (2007). The Neolithic Background. In P. M. Day & R. C. P. Doonan (Eds.), *Metalurgy in the Early Bronze Age Aegean* (Vol. 7, pp. 168–206). Sheffield studies in Aegean archaeology.
- Zaikov, V.V., Zaikova, E.V., Yuminov, A.M., 2009. Osmium inclusions in ancient gold products. *Doklady Earth Sciences* 432 (1), 593–597. <https://doi.org/10.1134/S1028334X10050090>.
- Zaykov, V.V., Kotlyarov, V.A., Zaykova, E.V., Melekestseva, I.Y.U., 2017. The Phenomenon of the Influence of Gold Melt on Microinclusions of platinum Group Minerals in Ancient Gold Objects. *Archaeometry* 59 (1), 96–104. <https://doi.org/10.1111/arcm.12234>.
- Zaykov, V.V., Melekestseva, I.Y., Zaykova, E.V., Fellenger, D., Motz, D., 2018. Trace elements in Ancient Gold Products with PGE Microinclusions from Archaeological Sites of the urals and North Black Sea Region: LA-ICP-MS Data. *Archaeometry* 60 (6). <https://doi.org/10.1111/arcm.12381>.
- Zwicker, U., 1998. An investigation of inclusions of platinum-group metals in ancient coinage. *Metall. Numis.* 4, 171–201.